Chemistry of (Auracarborane)(alkylidyne)tungsten and -molybdenum Compounds: Flexible Metal Cluster Molecules and Gold–Proton Exchange Processes on Carborane Cages†

John C. Jeffery,[1a] Paul A. Jelliss,[1a,b] and F. Gordon A. Stone*,[1b]

School of Chemistry, The University, Bristol BS8 1TS, U.K., and Department of Chemistry, Baylor University, Waco, Texas 76798-7348

Received March 4, 1994®

Treatment of the species Tl[10-*endo*-{Au(tht)}-7,8-Me_2-*nido*-7,8-$C_2B_9H_9$] (**1c**) (tht = tetrahydrothiophene) in thf (tetrahydrofuran) at −78 °C with the alkylidyne complexes [M(≡CR)-$(CO)_2(\eta$-$C_5H_5)$] (M = W, R = C_6H_4Me-4 (**2a**); M = Mo, R = C_6H_4Me-4 (**2b**); M = W, R = $C_6H_3Me_2$-2,6 (**2c**)) followed by addition of [NEt_4]Cl gave respectively the salts [NEt_4]$_2$[10,-10′-*endo*-{Au_2M(μ_3-CC_6H_4Me-4)$(CO)_2(\eta$-$C_5H_5)$}-7,7′,8,8′-Me_4-*nido*-7,7′,8,8′-$(C_2B_9H_9)_2$] (M = W (**3a**), Mo (**3b**)) and [NEt_4][10-*endo*-{AuW(μ-$CC_6H_3Me_2$-2,6)$(CO)_2(\eta$-$C_5H_5)$}-7,8-Me_2-*nido*-7,8-$C_2B_9H_9$] (**8**). The structure of the latter complex was determined by X-ray diffraction. Crystals are monoclinic, space group $P2_1/c$ with a = 8.741(3) Å, b = 21.100(5) Å, c = 19.300(5) Å, β = 98.33(2)°, and Z = 4. The anion consists of a *nido*-C_2B_9 carborane cage σ-bonded to an *endo*-gold atom via the boron atom β to the carbon atoms in the CCB*B*B face of the cage [Au—B(4) = 2.15(1) Å] and with additional weak contacts between the gold atom and the α-boron atoms [Au—B(3) = 2.51(1), Au—B(5) = 2.42(1) Å]. The Au—W bond [2.697(1) Å] is bridged asymmetrically by a μ-$CC_6H_3Me_2$-2,6 group [Au—C(60) = 2.11(1), W—C(60) = 1.91(1) Å]. Protonation of the three salts **3a,b** and **8** with HBF_4·Et_2O in thf at −78 °C yielded the complexes [9,9′-*exo*-{Au_2M(μ_3-CC_6H_4Me-4)$(CO)_2(\eta$-$C_5H_5)$}-7,7′,8,8′-Me_4-*nido*-7,7′,8,8′-$(C_2B_9H_{10})_2$] (M = W (**10a**), Mo (**10b**)) and [9-*exo*-{AuW(μ-$CC_6H_3Me_2$-2,6)$(CO)_2(\eta$-$C_5H_5)$}-7,8-Me_2-*nido*-7,8-$C_2B_9H_{10}$] (**12**), respectively. The crystal structure of the digold—tungsten species **10a** was determined by X-ray diffraction. Crystals are monoclinic, space group $P2_1/c$ with a = 16.676(4) Å, b = 13.879(5) Å, c = 18.260(6) Å, β = 90.90(2)°, and Z = 4. The molecule has a tetrahedral μ_3-CAu_2W core [W—Au(1) = 2.710(1), W—Au(2) = 2.727(1), Au(1)—Au(2) = 3.049(2), W—C(60) = 2.00-(2), Au(1)—C(60) = 2.10(2), Au(2)—C(60) = 2.11(3) Å] with *nido*-C_2B_9 carborane cages bonded to each gold atom via strong Au—B_α (average 2.17 Å) and weaker Au—B_β (average 2.62 Å) contacts. The complexes **10a,b** and **12** display dynamic behavior in solution, as revealed by variable temperature NMR studies. The reaction of the salt **3a** in thf with [$Rh_2(\mu$-$Cl)_2(CO)_4$] and with [*cis*-$IrCl(CO)_2(NH_2C_6H_4$Me-4)], in the presence of $TlBF_4$, afforded the complexes [$WM_2Au_2(\mu_3$-CC_6H_4Me-4)$(CO)_6(\eta$-$C_5H_5)(\eta^5$-7,8-Me_2-7,8-$C_2B_9H_9)_2$] (M = Rh (**6**), Ir (**14**)) as a result of cage transfer from gold to rhodium and to iridium, respectively. The NMR data (^{1}H, ^{13}C{^{1}H}, and ^{11}B{^{1}H}) for the new compounds are reported and discussed in relation to the structures.

Introduction

The salts [NEt_4][10-*endo*-Au(PPh_3)-7,8-R_2-*nido*-7,8-$C_2B_9H_9$] (R = Me (**1a**), H(**1b**)) have proven useful reagents in the synthesis of metallacarborane complexes containing gold bonded to rhodium,[2a] iridium,[2b] platinum,[2c] or other gold atoms.[2d] With a view to extending research in this area, we have prepared the new auracarborane reagent Tl[10-*endo*-Au(tht)-7,8-Me_2-*nido*-7,8-$C_2B_9H_9$] (tht = tetrahydrothiophene) (**1c**) in situ and have studied its reactions with the alkylidyne(cyclopentadienyl)metal complexes [M(≡CR)$(CO)_2(\eta$-$C_5H_5)$] (M = W, Mo, R = aryl). It is well established that labile ligands in organometal complexes are readily displaced by the C≡M bonds of the species [M(≡CR)$(CO)_2(\eta$-$C_5H_5)$] to afford homo- and heterometallic cluster complexes.[3]

Results and Discussion

Treatment of a suspension of Tl[*closo*-1,2-Me_2-3,1,2-$TlC_2B_9H_9$][4] in thf (thf = tetrahydrofuran) at −78 °C with [AuCl(tht)], followed by addition of PPh_3 and [NEt_4]Cl

* To whom correspondence should be addressed.

† Several new compounds reported herein contain [7,8-Me_2-*nido*-7,8-$C_2B_9H_9$]$^{2-}$ ligands, with gold atoms essentially σ-bonded to the carborane cage and the twelfth vertex considered absent. However, when a metal vertex is present, resulting in a *closo*-icosahedral system, it is convenient to retain the *nido* nomenclature *i.e.* [η^5-7,8-Me_2-7,8-$C_2B_9H_9$]$^{2-}$, with the cage related to a cyclopentadienyl ligand.

® Abstract published in *Advance ACS Abstracts*, May 15, 1994.

(1) (a) University of Bristol. (b) Baylor University.

(2) (a) Jeffery, J. C.; Jelliss, P. A.; Stone, F. G. A. *J. Chem. Soc., Dalton Trans.* **1993**, 1073. (b) Jeffery, J. C.; Jelliss, P. A.; Stone, F. G. A. *J. Chem. Soc., Dalton Trans.* **1993**, 1083. (c) Jeffery, J. C.; Jelliss, P. A.; Stone, F. G. A. *Inorg. Chem.* **1993**, *32*, 3943. (d) Jeffery, J. C.; Jelliss, P. A.; Stone, F. G. A. *J. Chem. Soc., Dalton Trans.* **1994**, 25.

(3) (a) Stone, F. G. A. *Angew. Chem., Int. Ed. Engl.* **1984**, *23*, 89. (b) Stone, F. G. A. *Pure Appl. Chem.* **1986**, *58*, 529. (c) Stone, F. G. A. *Adv. Organomet. Chem.* **1990**, *31*, 53.

(4) (a) Spencer, J. L.; Green, M.; Stone, F. G. A. *J. Chem. Soc., Chem. Commun.* **1972**, 1178. (b) Manning, M. J.; Knobler, C. B.; Hawthorne, M. F.; Do, Y. *Inorg. Chem.* **1991**, *30*, 3589. (c) Jutzi, P.; Wegener, D.; Hursthouse, M. B. *Chem. Ber.* **1991**, *124*, 295.

0276-7333/94/2313-2651$04.50/0

Table 1. Analytical and Physical Data

compd	color	yield/%	ν_{max}(CO)[a]/cm^{-1}	anal./%[b] C	H	N
3a, $[NEt_4]_2$[10,10′-*endo*-{$Au_2W(\mu_3$-CC_6H_4Me-4)-$(CO)_2(\eta$-$C_5H_5)$}-7,7′,8,8′-Me_4-*nido*-7,7′,8,8′-$(C_2B_9H_9)_2$]	deep red	90[c]	2006 (s), 1949 (s)	35.3[d] (35.4)	6.3 (6.3)	1.9 (1.9)
3b, $[NEt_4]_2$[10,10′-*endo*-{$Au_2Mo(\mu_3$-CC_6H_4Me-4)-$(CO)_2(\eta$-$C_5H_5)$}-7,7′,8,8′-Me_4-*nido*-7,7′,8,8′-$(C_2B_9H_9)_2$]	deep red	76	2010 (s), 1957 (s)	37.0 (36.2)	6.5 (6.4)	2.2 (2.2)
8, $[NEt_4]$[10-*endo*-{$AuW(\mu$-$CC_6H_3Me_2$-2,6)$(CO)_2$-$(\eta$-$C_5H_5)$}-7,8-Me_2-*nido*-7,8-$C_2B_9H_9$]	deep orange	91	2005 (vs), 1939 (vs)	36.9 (37.0)	5.7 (5.4)	1.5 (1.5)
10a, [9,9′-*exo*-{$Au_2W(\mu_3$-CC_6H_4Me-4)$(CO)_2$-$(\eta$-$C_5H_5)$}-7,7′,8,8′-Me_4-*nido*-7,7′,8,8′-$(C_2B_9H_{10})_2$]	yellow	64	2055 (s), 2004 (s)	23.6 (24.6)	4.1 (3.9)	
10b, [9,9′-*exo*-{$Au_2Mo(\mu_3$-CC_6H_4Me-4)$(CO)_2$-$(\eta$-$C_5H_5)$}-7,7′,8,8′-Me_4-*nido*-7,7′,8,8′-$(C_2B_9H_{10})_2$]	yellow	71	2059 (s), 2018 (s)	25.8 (26.6)	4.6 (4.3)	
12, [9-*exo*-{$AuW(\mu$-$CC_6H_3Me_2$-2,6)$(CO)_2$-$(\eta$-$C_5H_5)$}-7,8-Me_2-*nido*-7,8-$C_2B_9H_{10}$]	yellow	77	2026 (vs), 1965 (vs)	31.6 (30.8)	4.1 (3.9)	
14, $[WIr_2Au_2(\mu_3$-CC_6H_4Me-4)$(CO)_6(\eta$-$C_5H_5)$-$(\eta^5$-7,8-Me_2-7,8-$C_2B_9H_9)_2$]	yellow	34	2049 (s), 2010 (sh), 1995 (s), 1950 (m)	21.0 (20.0)	3.0 (2.6)	

[a] Measured in CH_2Cl_2; medium-intensity broad bands observed at ca. 2550 cm^{-1} in the spectra of all the compounds are due to B–H absorptions. [b] Calculated values are given in parentheses. [c] Yield is 86% when prepared from **7** and Tl[*closo*-1,2-Me_2-3,1,2-$TlC_2B_9H_9$]. [d] Crystallizes with one molecule of Et_2O.

yielded the previously reported salt **1a**.[2a] It was apparent

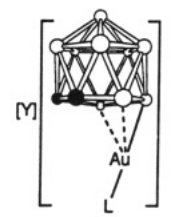

○ BH

	Y	L	●
1a	NEt_4	PPh_3	CMe
1b	NEt_4	PPh_3	CH
1c	Tl	tht	CMe

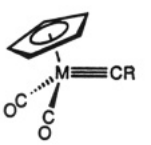

2a	W	C_6H_4Me-4
2b	Mo	C_6H_4Me-4
2c	W	$C_6H_3Me_2$-2,6

that prior to addition of PPh_3 a reactive intermediate had formed in solution. Bright orange in color, this species is unstable in solution above ca. −65 °C, and although uncharacterized, is reasonably formulated as the salt Tl-[10-*endo*-{Au(tht)}-7,8-Me_2-*nido*-7,8-$C_2B_9H_9$] (**1c**), a structural analog of **1a**.

Addition of [M(≡CC_6H_4Me-4)$(CO)_2(\eta$-$C_5H_5)$] (M = W (**2a**), Mo (**2b**)) to thf solutions of **1c** at −78 °C, followed by addition of $[NEt_4]Cl$, gave in high yield the intensely deep red salts $[NEt_4]_2$[10,10′-*endo*-{$Au_2M(\mu_3$-CC_6H_4Me-4)$(CO)_2(\eta$-$C_5H_5)$}-7,7′,8,8′-Me_4-*nido*-7,7′,8,8′-$(C_2B_9H_9)_2$] (M = W (**3a**), Mo (**3b**)), formed by displacement of tht from the gold in the precursor **1c**. The salts **3a** and **3b** were fully characterized by the data listed in Tables 1 and 2.

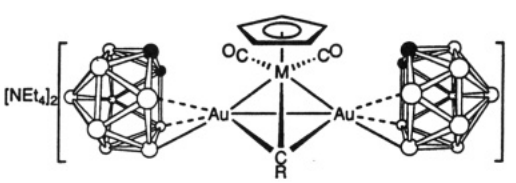

M	
3a	W
3b	Mo

○ BH ● CMe
R = C_6H_4Me-4

Unfortunately, crystals of **3a** of sufficient quality for an X-ray diffraction study could not be grown. However, the limited data obtained revealed the metal core structure depicted. The placement of the two gold atoms with respect to the carborane groups in this dianionic complex is thus apparently similar to that found in the structures of the complexes [5,10-*exo*-{$Rh(PPh_3)_2$}-5,10-$(\mu$-H$)_2$-10-*endo*-{$Au(PPh_3)$}-7,8-Me_2-*nido*-7,8-$C_2B_9H_7$] (**4**)[2a] and [10-

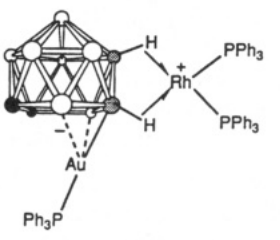

4

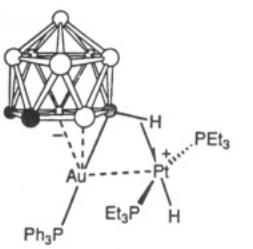

5

○ BH ● B ● CMe

exo-{$Pt(H)(PEt_3)_2$}-10-$(\mu$-H)-10-*endo*-{$Au(PPh_3)$}-7,8-Me_2-*nido*-7,8-$C_2B_9H_8$] (**5**),[2c] which also have their gold atoms bound strongly to the boron atom β to the carbon atoms in the open CCB*B*B face of the cage, with weaker attachments to the α-boron atoms. Interestingly, the μ_3-CAu_2W core of **3a** is also present in the cluster [$WRh_2Au_2(\mu_3$-CC_6H_4Me-4)$(CO)_6(\eta$-$C_5H_5)(\eta^5$-7,8-Me_2-7,8-$C_2B_9H_9)_2$] (**6**), the structure of which has been established by X-ray crystallography.[5]

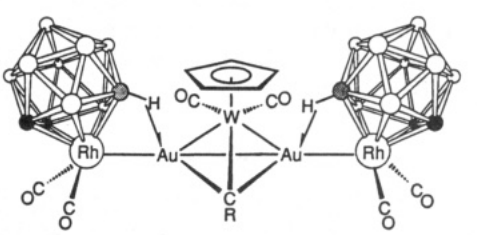

6

○ BH ● B ● CMe
R = C_6H_4Me-4

The IR spectra of the salts **3** show carbonyl absorptions at frequencies (2006 (s), 1949 (s) (**3a**), 2010 (s), 1957 (s) cm^{-1} (**3b**)) higher than those of the respective precursor alkylidyne complexes (1984 (s), 1909 (s) (**2a**), 1994 (s), 1919 (s) cm^{-1} (**2b**); also measured in CH_2Cl_2),[6] indicating a lowering of electron density on the group 6 metal atom upon cluster formation. The NMR data (^{1}H, ^{13}C{^{1}H}, and

(5) Carr, N.; Gimeno, M. C.; Goldberg, J. E.; Pilotti, M. U.; Stone F. G. A.; Topaloğlu, I. *J. Chem. Soc., Dalton Trans.* **1990**, 2253.
(6) Fischer, E. O.; Lindner, T. L.; Huttner, G.; Friedrich, P.; Kreissl, F. R.; Besenhard, J. O. *Chem. Ber.* **1977**, *110*, 3397.

Table 2. Hydrogen-1, Carbon-13, and Boron-11 NMR Data[a]

compd	$^1H/\delta^b$	$^{13}C/\delta^c$	$^{11}B/\delta^d$
3a	1.18 (t, 24 H, CH_2Me, J(HH) = 6), 1.55, 1.65 (s × 2, 12 H, CMe), 2.38 (s, 3 H, Me-4), 3.03 (q, 16 H, NCH_2, J(HH) = 6), 6.07 (s, 5 H, C_5H_5), 7.12, 8.06 {$(AB)_2$, 4 H, C_6H_4, J(AB) = 8}	239.6 (br, μ_3-C), 212.7 (CO, J(WC) = 162), 149.9 [$C^1(C_6H_4)$], 137.0, 130.4, 127.9 (C_6H_4), 90.1 (C_5H_5), 55.5 (vbr, *C*Me), 53.0 (NCH_2), 23.8, 23.1 (*CMe*), 21.1 (Me-4), 7.9 (CH_2Me)	−11.3 (2 B), −14.3 (2 B), −16.1 (6 B), −18.7 (2 B), −20.2 (2 B), −22.5 (2 B), −34.6 (2 B)
3b	1.17 (t, 24 H, CH_2Me, J(HH) = 6), 1.59, 1.62 (s × 2, 12 H, CMe), 2.36 (s, 3 H, Me-4), 3.03 (q, 16 H, NCH_2, J(HH) = 6), 6.02 (s, 5 H, C_5H_5), 7.10, 8.12 {$(AB)_2$, 4 H, C_6H_4, J(AB) = 8}	[e]253.4 (br, μ_3-C), 225.5 (CO), 148.9 [$C^1(C_6H_4)$], 137.2, 131.0, 128.1 (C_6H_4), 92.6 (C_5H_5), 53.0 (NCH_2), 24.0, 23.2 (*CMe*), 21.2 (Me-4), 7.8 (CH_2Me)	−9.4 (2 B), −12.3 (2 B), −13.7 (6 B), −17.0 (2 B), −18.5 (2 B), −20.7 (2 B), −32.4 (2 B)
8	1.24 (t of t, 12 H, CH_2Me, J(HH) = 8, J(NH) = 2), 1.38 (s, 6 H, CMe), 2.37 (s, 6 H, Me_2-2,6), 3.13 (q, 8 H, NCH_2, J(HH) = 8), 5.77 (s, 5 H, C_5H_5), 6.99 (m, br, 3 H, C_6H_3)	288.6 (μ-C, J(WC) = 152), 217.6 (CO, J(WC) = 183), 153.4 [$C^1(C_6H_3)$], 133.5, 127.5, 126.8 (C_6H_3), 91.7 (C_5H_5), 55.0 (br, *C*Me), 53.0 (NCH_2), 22.9, 21.4 (*CMe* and Me_2-2,6), 7.7 (CH_2Me)	−12.0 (1 B), −14.9 (1 B), −17.1 (2 B), −18.1 (2 B), −19.4 (2 B), −34.8 (1 B)
10a[f]	−2.6 (vbr, 2 H, H_{endo}), 1.29 (s, 3 H, CMe), 1.50 (s, 6 H, CMe),[g] 1.75 (s, 3 H, CMe), 2.50 (s, 3 H, Me-4), 6.19 (s, 5 H, C_5H_5), 7.37, 7.60 {$(AB)_2$, 4 H, C_6H_4, J(AB) = 8}	238.0 (br, μ_3-C), 203.8 (CO, J(WC) = 169), 203.5 (CO, J(WC) = 164), 146.8 [$C^1(C_6H_4)$], 142.4, 130.7, 130.0 (C_6H_4), 91.3 (C_5H_5), 71.5 (vbr, *C*Me), 22.6, 22.5, 22.2, 21.8 (*CMe*), 21.7 (Me-4)	−7.3 (vbr, 4 B), −11.5 (vbr, 2 B), −14.7 (vbr, 8 B), −28.4 (vbr, 2 B), −32.9 (vbr, 2 B)
10b[h]	−2.6 (vbr, 2 H, H_{endo}), 1.16, 1.36, 1.43, 1.68 (s × 4, 12 H, CMe), 2.42 (s, 3 H, Me-4), 6.06 (s, 5 H, C_5H_5), 7.28, 7.54 {$(AB)_2$, 4 H, C_6H_4, J(AB) = 8}	253.0 (br, μ_3-C), 217.4, 216.9 (CO), 145.1 [$C^1(C_6H_4)$], 142.0, 130.5, 129.3 (C_6H_4), 93.1 (C_5H_5), 70.9 (vbr, *C*Me), 21.9, 21.7, 21.5 (*CMe*), 21.1 (Me-4), 20.9 (*CMe*)	−5.4 (vbr, 4 B), −9.6 (vbr, 2 B), −12.7 (vbr, 8 B), −26.1 (vbr, 2 B), −30.9 (vbr, 2 B)
12[i]	−2.6 (vbr, 1 H, H_{endo}), 1.42, 1.57 (s × 2, 6 H, CMe), 2.31, 2.35 (s × 2, 6 H, Me_2-2,6), 5.97 (s, 5 H, C_5H_5), 7.17, 7.27 (AB_2, 3 H, C_6H_3, J(AB) = 8)	278.4 (μ-C, J(WC) = 146), 211.7 (CO, J(WC) = 174), 211.5 (CO, J(WC) = 170), 150.4 [$C^1(C_6H_3)$], 136.4, 135.4, 129.5, 128.2 (C_6H_3), 92.5 (C_5H_5), 70.8 (vbr, *C*Me), 22.7 (*CMe*), 22.0 (Me_2-2,6), 21.8 (*CMe*), 21.7 (Me_2-2,6)	−8.4 (2 B), −12.1 (1 B), −15.8 (4 B), −27.7 (1 B), −33.8 (1 B)
14	[j]2.42 (s, 3 H, Me-4), 2.52, 2.58 (s × 2, 12 H, CMe), 5.97 (s, 5 H, C_5H_5), 7.22, 7.57 {$(AB)_2$, 4 H, C_6H_4, J(AB) = 8}	242.1 (br, μ_3-C), 205.8 (WCO, J(WC) = 164), 172.6, 172.5 (IrCO), 148.7 [$C^1(C_6H_4)$], 140.9, 129.9, 129.3 (C_6H_4), 90.8 (C_5H_5), 70.8, 69.6 (br, *C*Me), 32.7, 30.1 (*CMe*), 21.5 (Me-4)	−1.6 (1 B), −3.6 (1 B), −11.5 (1 B), −11.8 (1 B), −13.9 (vbr, 5 B)

[a] Chemical shifts (δ) in ppm, coupling constants (J) in Hz, measurements in CD_2Cl_2, and at room temperature unless otherwise stated. [b] Resonances for terminal BH protons occur as broad unresolved signals in the range δ ca. −2 to +3. [c] Hydrogen-1 decoupled; chemical shifts are positive to high frequency of $SiMe_4$. Spectra of **3a,b**, **8**, and **10a,b** reveal only one very broad, unresolved resonance for cage *C*Me nuclei despite the inequivalence of the CMe groups. [d] Hydrogen-1 decoupled; chemical shifts are positive to high frequency of $BF_3{\cdot}Et_2O$ (external). All resonances are broad, with some signals corresponding to overlapping peaks which do not necessarily indicate symmetry equivalence. [e] Due to low solubility and probable peak broadness, resonances due to *C*Me nuclei could not be identified for samples measured in CD_2Cl_2 or thf-d_8. [f] ^1H and $^{13}C\{^1H\}$ spectra measured at −70 °C. [g] Coincidence of two singlet peaks; see text. [h] ^1H and $^{13}C\{^1H\}$ spectra measured at −80 °C. [i] ^1H and $^{13}C\{^1H\}$ spectra measured at −90 °C. [j] Measured at −20 °C.

$^{11}B\{^1H\}$) for **3a** are given in Table 2. From the ^1H NMR spectrum peak integrals indicate the presence of two carborane cages. Although a plane of symmetry lies through the tungsten and μ_3-C atoms and the midpoint of the Au–Au connectivity, this is insufficient to make the two methyl groups on any one of the carborane cages equivalent. Thus there are two signals in the ^1H NMR spectrum at δ 1.55 and 1.65 and two signals in the $^{13}C\{^1H\}$ NMR spectrum at δ 23.8 and 23.1 for the C*Me* groups. The signal arising from the vertex carbon nuclei (*C*Me) is observed as a very broad unresolved peak at δ 55.5. The above mentioned symmetry plane does render the tungsten carbonyl groups equivalent, and one resonance is observed in the $^{13}C\{^1H\}$ NMR spectrum at δ 212.7 (J(WC) = 162 Hz). Also in this spectrum, a broad peak at δ 239.6 is assigned to the μ_3-*C*C_6H_4Me-4 nucleus. This is a relatively low chemical shift for a μ_3-alkylidyne carbon atom and is to be compared with the chemical shift of the μ_3-C nucleus in complex **6**, which resonates at δ 289.3.[5] The $^{11}B\{^1H\}$ NMR spectrum of **3a** revealed broad overlapping peaks in the range δ-11.3 to −34.6 and is relatively uninformative.

The NMR spectral data for complex **3b** are in accord with a structure similar to that of **3a**. Of note is the μ_3-*C*C_6H_4Me-4 resonance in the $^{13}C\{^1H\}$ NMR spectrum (δ 253.4), which is once more at a relatively low chemical shift for this type of bridging alkylidyne carbon atom.

The formation of the trinuclear species **3a** is perhaps surprising when compared with the reaction of **2a** with [AuCl(tht)], which gives the dinuclear metal complex [WAuCl(μ-CC_6H_4Me-4)(CO)$_2$(η-C_5H_5)] (**7**).[7] When complex **7** was treated with 1 equiv of Tl[*closo*-1,2-Me_2-3,1,2-$TlC_2B_9H_9$] in thf, followed by addition of $[NEt_4]Cl$, a 1:1 mixture of **2a** and **3a** was formed. The former was readily separated by extraction with Et_2O, and the latter was purified and identified by its IR and ^1H NMR spectra. The synthesis of **3a** from **7** was monitored by periodic IR spectroscopic measurements of the solution containing the reactants. From this it was evident that formation of **3a** proceeded via the intermediacy of a gold–tunsgten thallium salt of probable structure **A** (Scheme 1), giving rise to carbonyl bands observed briefly in the IR at 1993 (vs) and 1929 (vs) cm^{-1}, before converting to the salt **B**, having the μ_3-CAu_2W core and showing bands at 2013 (s) and 1959 (s) cm^{-1}.

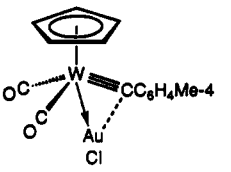

7

When the products **3** are formed from **2a,b** the reagent **1c** displays behavior similar to that of [Cu(thf)(η-C_5Me_5)] in that reaction of the latter with **2a** also affords a trinuclear metal complex, [WCu_2(μ_3-CC_6H_4Me-4)(CO)$_2$(η-C_5H_5)(η-

(7) Gimeno, M. C.; Stone, F. G. A. *J. Chem. Soc., Dalton Trans.* **1990**, 2239.

Scheme 1. Formation of 3a through the Intermediacy of a Dinuclear Species[a]

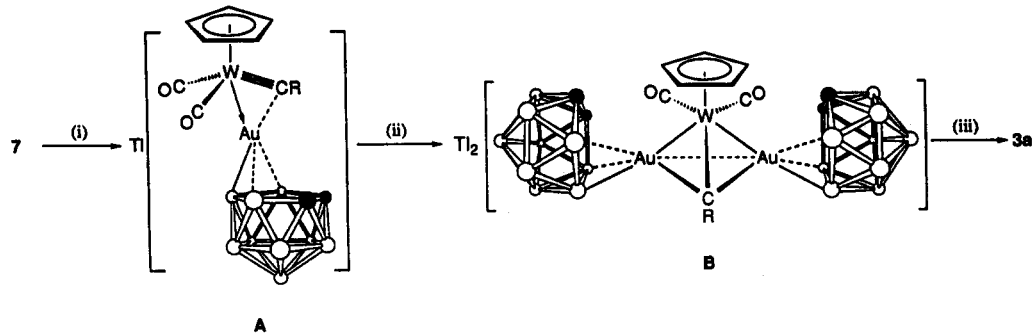

[a] Key: (i) Tl[*closo*-1,2-Me_2-3,1,2-$TlC_2B_9H_9$], thf solvent; (ii) dissociation into **2a** and Tl[10-*endo*-{Au(thf)}-7,8-Me_2-*nido*-7,8-$C_2B_9H_9$], with recombination in a 1:2 ratio (see text); (iii) $[NEt_4]Cl$.

$C_5Me_5)_2$].[8a] This is in contrast with observations employing other metal–ligand groups which, even when used in excess, react with complexes such as **2a** to give dimetal rather than trimetal complexes.[3,7,8a] However, it has been shown[8b] that reaction of [W(≡$CC_6H_3Me_2$-2,6)$(CO)_2(\eta$-$C_5H_5)$] (**2c**), containing the bulky $CC_6H_3Me_2$-2,6 group, with a solution of [Cu(thf)$(\eta$-$C_5Me_5)$] gives the dimetal complex [WCu$(\mu$-$CC_6H_3Me_2$-2,6)$(CO)_2(\eta$-$C_5H_5)(\eta$-$C_5Me_5)$] and not a trimetal species. Similar reactivity patterns have been observed in reactions between [W(≡CR)$(CO)_2$-$(\eta$-$C_5H_5)$] (R = C_6H_4Me-4, C_6H_4Me-2, or $C_6H_3Me_2$-2,6) and $[Fe_2(CO)_9]$.[9] Formation of trimetal species with μ_3-CFe_2W cores was less favored if the aryl groups had substituents *ortho* to the ligating alkylidyne carbon atom.

With these results in mind, the reagent **1c** was treated with **2c** in thf at −78 °C, and $[NEt_4]Cl$ was added. This reaction gave a dimetal complex characterized as $[NEt_4]$-[10-*endo*-{AuW$(\mu$-$CC_6H_3Me_2$-2,6)$(CO)_2(\eta$-$C_5H_5)$}-7,8-Me_2-*nido*-7,8-$C_2B_9H_9$] (**8**). Before the IR and NMR spectroscopic data for **8** are discussed, the results of an X-ray diffraction study are presented (see Table 3 and Figure 1).

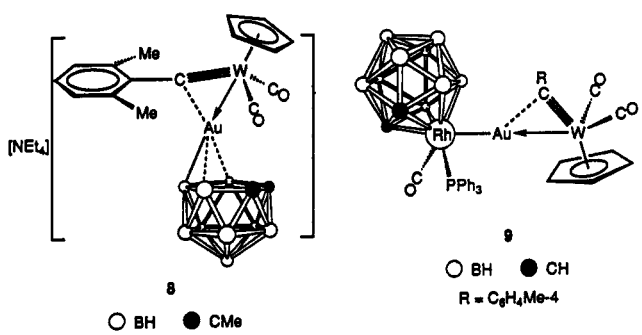

The anion has a bent W–Au–B(4) spine [150.2(3)°]. The gold atom is essentially σ-bonded to the *nido*-icosahedral fragment at the boron atom B(4) with Au—B(4) = 2.15(1) Å. However, there are also weaker contacts to the α-boron atoms of the cage face [Au—B(3) = 2.51(1), Au—B(5) = 2.42(1) Å] with slight slippage toward B(5), again similar to those observed in the structures of the complexes **4** and **5**. The Au—W bond [2.697(1) Å] is spanned asymmetrically by the 2,6-xylylmethylidyne ligand [W—C(60) = 1.91(1), Au–C(60) = 2.11(1) Å], a feature observed with the 4-tolylmethylidyne group in the structure of the complex [WRhAu$(\mu$-CC_6H_4Me-4)$(CO)_3(PPh_3)(\eta$-$C_5H_5)(\eta^5$-7,8-$C_2B_9H_{11}$)] (**9**),[5] and which has the corresponding bond distances Au–W = 2.732(1), W—μ-C = 1.90(1), and Au—μ-C = 2.13(1) Å.

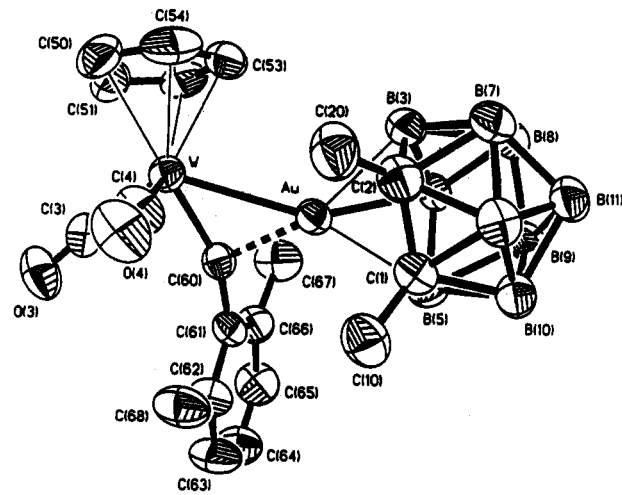

Figure 1. Structure of the anion of $[NEt_4]$[10-*endo*-{AuW$(\mu$-$CC_6H_3Me_2$-2,6)$(CO)_2(\eta$-$C_5H_5)$}-7,8-Me_2-*nido*-7,8-$C_2B_9H_9$] (**8**), showing the crystallographic labeling scheme. Thermal ellipsoids are shown at the 40% probability level.

A bonding description given for the W$(\mu$-C)Au ring in **9**, which accounts for asymmetric bridging of the CC_6H_4-Me-4 group while at the same time maintaining reasonable electron counts at the two metal centers, invoked a W→Au two-electron donor bond and a Rh—Au single bond.[5] This results in a 14-electron gold(I) center, as is commonly found. In the new complex **8**, the boron atom B(4) of the carborane cage formally replaces the rhodium atom of **9** as a one-electron donor. The weak Au—μ-C interactions in **8** and **9** provide a mechanism for transfer of electron density from gold to the π^* orbitals of the W≡C systems, although such an interaction may be partially offset in **8** by the acceptance of electron density from a frontier orbital on the carborane cage face into the energetically high-lying gold 6p orbitals.[10] The somewhat asymmetric bridging of the 2,6-xylylmethylidyne bridge in **8** is reflected in the angle W—C(60)—C(61) [158.2(8)°], which is very similar to that observed for the W—μ-C—C^1(aryl) angle in complex **9** [156(1)°].[5]

The IR spectrum of **8** shows CO stretching bands at 2005 (vs) and 1939 (vs) cm^{-1}. These frequencies, along

(8) (a) Carriedo, G. A.; Howard, J. A. K.; Stone, F. G. A. *J. Chem. Soc., Dalton Trans.* **1984**, 1555 and references therein. (b) Dossett, S. J.; Hill, A. F.; Howard, J. A. K.; Nasir, B. A.; Spaniol, T. P.; Sherwood, P.; Stone, F. G. A. *J. Chem. Soc., Dalton Trans.* **1989**, 1871.

(9) (a) Baumann, F.-E.; Howard, J. A. K.; Johnson, O.; Stone, F. G. A. *J. Chem. Soc., Dalton Trans.* **1987**, 2917. (b) Baumann, F.-E.; Howard, J. A. K.; Musgrove, R. J.; Sherwood, P.; Stone, F. G. A. *J. Chem. Soc., Dalton Trans.* **1988**, 1879. (c) Dossett, S. J.; Hill, A. F.; Jeffery, J. C.; Marken, F.; Sherwood, P.; Stone, F. G. A. *J. Chem. Soc., Dalton Trans.* **1988**, 2453.

(10) Hamilton, E. J. M.; Welch, A. J. *Polyhedron* **1990**, *9*, 2407.

Table 3. Selected Internuclear Distances (Å) and Angles (deg) for 8, with Estimated Standard Deviations in Parentheses

Au–W	2.697(1)	Au–B(3)	2.51(1)	Au–B(4)	2.15(1)	Au–B(5)	2.42(1)
Au–C(60)	2.11(1)	W–C(3)	1.99(1)	W–C(4)	2.00(1)	W–C(60)	1.91(1)
C(1)–C(2)	1.58(2)	C(1)–B(5)	1.62(2)	C(1)–C(10)	1.51(2)	C(2)–B(3)	1.63(2)
C(2)–C(20)	1.49(2)	B(3)–B(4)	1.80(2)	B(4)–B(5)	1.90(2)	C(3)–O(3)	1.14(2)
C(4)–O(4)	1.13(2)	C(60)–C(61)	1.46(1)	C(61)–C(62)	1.41(2)	C(61)–C(66)	1.40(1)
C(62)–C(63)	1.39(2)	C(62)–C(68)	1.51(2)	C(63)–C(64)	1.35(2)	C(64)–C(65)	1.37(2)
C(65)–C(66)	1.40(2)	C(66)–C(67)	1.48(2)				
	W–C(C_5H_5)	2.31(2)–2.36(1)		C–C(C_5H_5)	1.37(3)–1.43(2)		
W–Au–B(3)	118.0(3)	W–Au–B(4)	150.2(3)	B(3)–Au–B(4)	44.5(4)		
W–Au–B(5)	159.8(3)	B(3)–Au–B(5)	69.6(4)	B(4)–Au–B(5)	48.7(4)		
W–Au–C(60)	44.7(3)	B(3)–Au–C(60)	162.7(4)	B(4)–Au–C(60)	149.9(4)		
B(5)–Au–C(60)	126.0(4)	Au–W–C(3)	127.9(4)	Au–W–C(4)	85.7(4)		
C(3)–W–C(4)	87.8(5)	Au–W–C(60)	51.0(3)	C(3)–W–C(60)	78.3(5)		
C(4)–W–C(60)	94.4(5)	Au–B(3)–C(2)	91.0(7)	Au–B(3)–B(4)	56.8(5)		
Au–B(4)–B(3)	78.6(6)	Au–B(4)–B(5)	73.2(6)	Au–B(5)–C(1)	93.6(7)		
Au–B(5)–B(4)	58.1(5)	W–C(3)–O(3)	176(1)	W–C(4)–O(4)	178(1)		
Au–C(60)–W	84.3(4)	Au–C(60)–C(61)	117.4(7)	W–C(60)–C(61)	158.2(8)		
C(60)–C(61)–C(62)	120.9(9)	C(60)–C(61)–C(66)	119.1(9)				

with the structure determination of **8**, lend credence to the proposed dinuclear structure of intermediate **A** (Scheme 1; ν_{max}(CO) 1993 (vs), 1929 (vs) cm^{-1}) on route to the salt **3a** discussed earlier. The semibridging nature of the arylmethylidyne ligand and the retention of triple bond character in the W≡C systems of **8** and **9** result in similar chemical shifts for the μ-C nuclei in their $^{13}C\{^1H\}$ NMR spectra (**8**, δ 288.6 (J(WC) = 152); **9**, δ 284.3 (J(WC) = 151 Hz)). Generally, signals for alkylidyne carbon atoms which bridge two metal centers are appreciably more deshielded than this.[9c] The ^1H NMR spectrum for **8** revealed one signal each due to the cage CMe and xylyl Me_2-2,6 groups at δ 1.38 and 2.37, respectively, the latter value being more typical of a xylyl methyl shift. In addition, the $^{13}C\{^1H\}$ NMR spectrum displayed one resonance for the CO groups (δ 217.6, J(WC) = 183 Hz), along with one broad resonance due to the cage *C*Me nuclei (δ 55.0) and two peaks at δ 22.9 and 21.4 due to the cage C*Me* and Me_2-2,6 groups. It can be inferred, therefore, despite the absence of a symmetry plane in the solid state structure of **8** (Figure 1), resulting in both cage CMe vertices lying on the same side of the plane W[C(60)]Au, that, in solution, the carbonyl, the xylyl methyl, and the cage methyl groups are respectively rendered equivalent. This can be achieved on the NMR time scale by rotation of the *nido*-C_2B_9 cage about the Au—B(4) bond or spinning of the W(μ-$CC_6H_3Me_2$-2,6)-$(CO)_2(\eta$-$C_5H_5)$ fragment about the Au—W bond, or both, depending on which of the weaker contacts, Au—C(60) or Au—B(3) and Au—B(5), are preferentially cleaved to facilitate such mobility. The remaining data, including the $^{11}B\{^1H\}$ NMR spectrum, are in accord with the above structural discussion.

Treatment of the complexes **3** with 2 equiv of HBF_4·Et_2O in thf at −78 °C produced the neutral complexes [9,9′-*exo*-{$Au_2M(\mu_3$-CC_6H_4Me-4)$(CO)_2(\eta$-$C_5H_5)$}-7,7′,8,8′-Me_4-*nido*-7,7′,8,8′-$(C_2B_9H_{10})_2$] (M = W (**10a**), Mo (**10b**)). Data

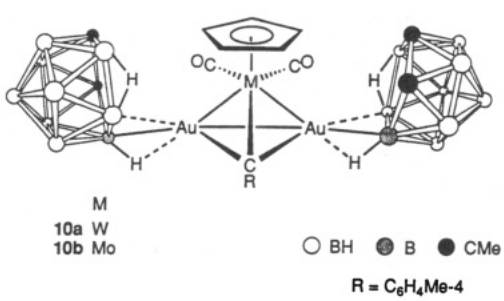

characterizing these new complexes are listed in Tables 1 and 2. Initially, the sites of protonation were unclear but, when reasonable quality crystals were obtained, the structure of **10a** was established by X-ray diffraction. The results are summarized in Table 4, and the molecular structure is shown in Figure 2.

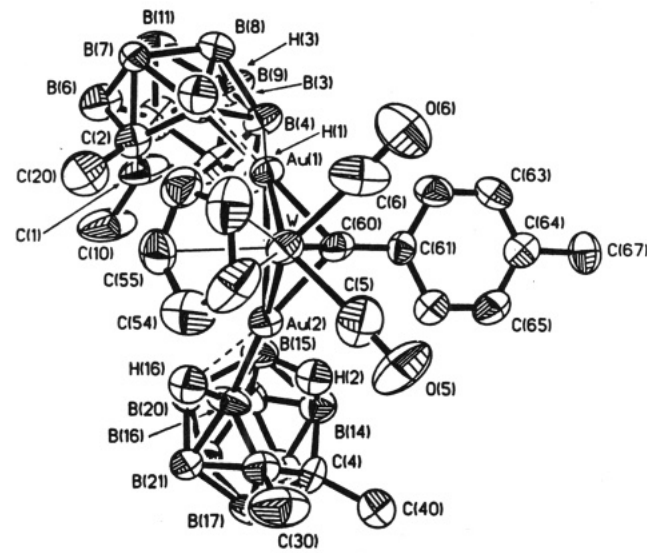

Figure 2. Structure of [9,9′-*exo*-{$Au_2W(\mu_3$-CC_6H_4Me-4)-$(CO)_2(\eta$-$C_5H_5)$}-7,7′,8,8′-Me_4-*nido*-7,7′,8,8′-$(C_2B_9H_{10})_2$] (**10a**), showing the crystallographic labeling scheme. Thermal ellipsoids are shown at the 30% probability level.

The metal core of **10a** consists of a WAu_2 triangle capped by a 4-tolylmethylidyne group [W—Au(1) = 2.710(1), W—Au(2) = 2.727(1), Au(1)—Au(2) = 3.049(2), W—C(60) = 2.00(2), Au(1)—C(60) = 2.10(2), Au(2)—C(60) = 2.11-(3) Å]. The Au—Au distance may be compared with the corresponding Au–Au bond length in complex **6** [2.969(2) Å],[5] which has a similar metal core. These contacts are both long, but they may still correspond to a significant electronic interaction between the gold atoms.[11] These distances in complexes **6** and **10a** are probably also influenced by the orbital and steric requirements of the bridging W(μ-CC_6H_4Me-4)$(CO)_2(\eta$-$C_5H_5)$ fragment.[12] The remaining distances in the core of **6** [W—Au = 2.755(2) and 2.744(2), W—μ-C = 2.02(2), Au—μ-C = 1.98(3) and 2.13(2) Å] compare very favorably with those of the new complex **10a**.

(11) Hall, K. P.; Mingos, D. M. P. *Prog. Inorg. Chem.* **1984**, *32*, 237.
(12) Elliot, G. P.; Howard, J. A. K.; Mise, T.; Moore, I.; Nunn, C. M.; Stone, F. G. A. *J. Chem. Soc., Dalton Trans.* **1986**, 2091.

Table 4. Selected Internuclear Distances (Å) and Angles (deg) for 10a, with Estimated Standard Deviations in Parentheses

W–Au(1)	2.710(1)	W–Au(2)	2.727(1)	W–C(5)	1.98(3)	W–C(6)	1.99(3)
W–C(60)	2.00(2)	Au(1)–Au(2)	3.049(2)	Au(1)–B(3)	2.17(2)	Au(1)–B(4)	2.61(2)
Au(1)–C(60)	2.10(2)	Au(2)–B(15)	2.62(3)	Au(2)–B(16)	2.17(2)	Au(2)–C(60)	2.11(3)
C(1)–C(2)	1.54(3)	C(1)–B(5)	1.68(5)	C(1)–B(6)	1.70(4)	C(1)–C(10)	1.54(3)
C(2)–B(3)	1.63(3)	C(2)–C(20)	1.48(3)	B(3)–B(4)	1.80(3)	B(3)–H(3)[a]	1.1(1)
B(4)–B(5)	1.92(5)	B(4)–H(1)	1.3(2)	B(5)–H(1)	1.2(2)	C(3)–C(4)	1.55(3)
C(3)–C(30)	1.55(4)	C(4)–B(14)	1.68(4)	C(4)–C(40)	1.54(3)	B(14)–B(15)	1.83(4)
B(14)–H(2)	1.3(2)	B(15)–B(16)	1.77(3)	B(15)–H(2)	1.3(2)	B(16)–H(16)[a]	1.1(1)
C(5)–O(5)	1.15(4)	C(6)–O(6)	1.15(4)	C(60)–C(61)	1.50(2)	C(64)–C(67)	1.53(2)
			W–C(C_5H_5)	2.31(2)–2.36(2)			
Au(1)–W–Au(2)	68.2(1)	Au(1)–W–C(5)	132.4(7)	Au(2)–W–C(5)	84.8(8)		
Au(1)–W–C(6)	85.3(8)	Au(2)–W–C(6)	133.9(7)	C(5)–W–C(6)	87(1)		
Au(1)–W–C(60)	50.2(5)	Au(2)–W–C(60)	50.3(5)	C(5)–W–C(60)	82.3(9)		
C(6)–W–C(60)	83.7(9)	W–Au(1)–Au(2)	56.2(1)	W–Au(1)–B(3)	144.8(5)		
Au(2)–Au(1)–B(3)	127.5(5)	W–Au(1)–B(4)	171.3(5)	Au(2)–Au(1)–B(4)	117.1(6)		
B(3)–Au(1)–B(4)	42.9(8)	W–Au(1)–C(60)	47.0(5)	Au(2)–Au(1)–C(60)	43.8(5)		
B(3)–Au(1)–C(60)	164.5(7)	B(4)–Au(1)–C(60)	124.6(8)	W–Au(2)–Au(1)	55.6(1)		
W–Au(2)–B(15)	163.5(5)	Au(1)–Au(2)–B(15)	108.7(5)	W–Au(2)–B(16)	153.9(6)		
Au(1)–Au(2)–B(16)	142.9(7)	B(15)–Au(2)–B(16)	42.2(8)	W–Au(2)–C(60)	46.6(5)		
Au(1)–Au(2)–C(60)	43.4(5)	B(15)–Au(2)–C(60)	119.4(7)	B(16)–Au(2)–C(60)	156.8(9)		
Au(1)–B(3)–C(2)	117(1)	Au(1)–B(3)–B(4)	82(1)	Au(1)–B(3)–H(3)	67(8)		
Au(1)–B(4)–B(3)	55.3(9)	Au(1)–B(4)–B(5)	116(2)	B(3)–B(4)–B(5)	100(2)		
Au(2)–B(15)–B(14)	119(2)	Au(2)–B(15)–B(16)	55(1)	B(14)–B(15)–B(16)	99(2)		
Au(2)–B(16)–C(3)	124(2)	Au(2)–B(16)–B(15)	83(1)	Au(2)–B(16)–H(16)	70(7)		
W–C(5)–O(5)	177(3)	W–C(6)–O(6)	176(2)	W–C(60)–Au(1)	82.8(7)		
W–C(60)–Au(2)	83.1(7)	Au(1)–C(60)–Au(2)	92.8(7)	W–C(60)–C(61)	149(1)		
Au(1)–C(60)–C(61)	118(1)	Au(2)–C(60)–C(61)	116(1)				

[a] Constrained lengths (see Experimental Section).

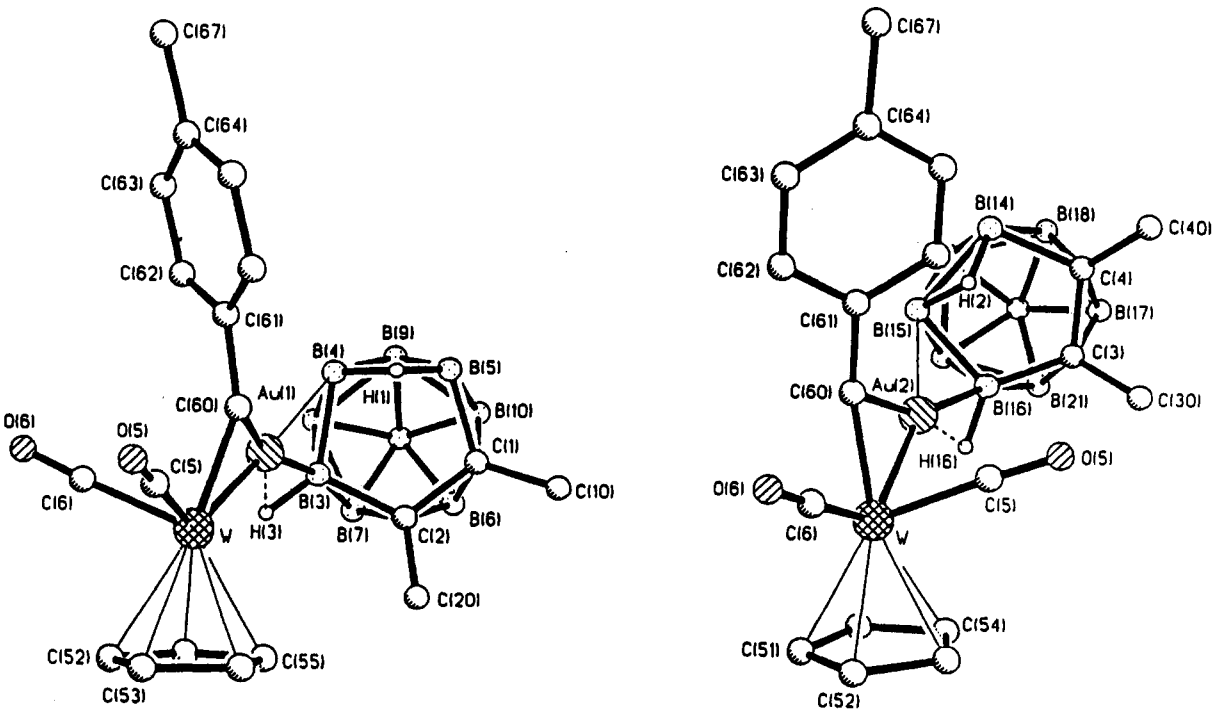

Figure 3. Views down onto the two carborane cage faces of complex **10a**, showing the apparent exopolyhedral disposition of the gold atoms with respect to the missing vertices of these cages.

The crystallographic analysis clearly revealed the sites of protonation as the faces of the two carborane cages. The hydrogen atoms H(1) and H(2) were both located in difference Fourier syntheses and occupy positions bridging the boron–boron connectivities B(4)—B(5) and B(14)—B(15), respectively. The gold atoms occupy essentially exopolyhedral positions with strong bonds to the cage face α-boron atoms [Au(1)—B(3) and Au(2)—B(16) = 2.17(2) Å]. Weaker attachments to the β-boron atoms were also observed with Au(1)—B(4) = 2.61(2) and Au(2)—B(15) = 2.62(3) Å. That the gold atoms sit just outside the polyhedral sphere of the carbon and boron vertices of both cages and are not directed toward the missing cage vertices is clearly seen in the two views shown in Figure 3. The question then arises as to whether there are any three-center two-electron B–H→Au interactions similar to that observed for the *exo*-gold atom in the digold complex [9-*exo*-{Au(PPh_3)}-9-(μ-H)-10-*endo*-{Au(PPh_3)}-7,8-Me_2-*nido*-7,8-$C_2B_9H_8$] (**11**).[2d] In complex **10a** the hydrogen atoms H(3) and H(16) bound to B(3) and B(16), respectively, were located in difference Fourier syntheses and though the Au···H distances seem initially too long for B–H→Au bonding [Au(1)···H(3) = 2.0(2) and Au(2)···H(16) = 2.1(1) Å], it is both possible and would not be surprising if there were some interaction. However, the NMR data discussed below did not reveal any evidence

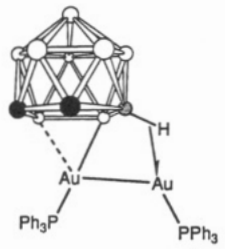

11

○ BH ◍ B ● CMe

of B–H→Au bonding. The disposition of either of the gold atoms relative to the faces of the cages is arguable. Although lying as if *exo*, it may be that the gold atoms are still contributing to cage cluster-counting as *endo* fragments but have been forced away from such positions by a combination of two effects: (i) overlap of the principal frontier orbital on the cage faces with the 1s orbitals of the *endo* protons H(1) and H(2),[10] a feature which would prevent strong contact between the gold atoms and the β-boron atoms; (ii) the weak B(3)–H(3)···Au(1) and B(16)–H(16)···Au(2) interactions, dragging the gold atoms further over the cage face edges. The two carborane cages are disposed asymmetrically with respect to a plane passing through W, C(60), and the midpoint of the Au(1)—Au(2) connectivity (Figure 2). The methyl groups on one cage are directed roughly opposite to those on the other, with one set of methyl groups (C(10) and C(20)) pointing in toward the aforementioned plane, the other set (C(30) and C(40)) away from it.

The IR spectrum of **10a** showed CO stretching bands at 2055 (s) and 2004 (s) cm^{-1}. The ^1H NMR spectrum recorded at −70 °C revealed only one very broad peak at δ −2.6 due to the *endo*-B–H–B protons (H(1) and H(2) in Figure 2). *Endo* protons bound to the face of a *nido*-icosahedral cage generally give rise to broad peaks in the range δ −2 to −5.[13] The spectrum also shows three signals at δ 1.29, 1.50, and 1.75 due to the cage CMe groups, although the peak at δ 1.50 integrates to two methyl groups and must be due to a fortuitous coincidence of two resonances. The $^{13}C\{^1H\}$ NMR spectrum measured at −70 °C displayed a single resonance at δ 238.0 due to the μ_3-C nucleus (C(60)), which is similar to that for the precursor **3a** (δ 239.6). There are two resonances due to the inequivalent CO ligands in **10a** at δ 203.8 and 203.5 (J(WC) = 169 and 164 Hz, respectively), and also revealed are four resonances arising from four inequivalent C*Me* nuclei at δ 22.6, 22.5, 22.2, and 21.8. The *C*Me nuclei only gave rise to an extremely broad unresolved and deshielded resonance at δ 71.5. These data imply an absence of symmetry planes in **10a**, thus rendering the methyl groups on all cages inequivalent, and similarly for the carbonyl ligands on the tungsten atom. The structure in solution at −70 °C is therefore equated with that observed in the totally asymmetric crystal structure discussed above (Figure 2). As stated above, there was no evidence in the ^1H NMR spectrum at this temperature for any B–H→Au groups, though occasionally these resonances cannot be detected, as was the case in the ^1H NMR spectrum of complex **6**.[5] Upon warming solutions of **10a** to 0 °C and measuring the ^1H NMR spectrum, the three signals due to the cage CMe groups collapse into two peaks at δ 1.52 and 1.53. The $^{13}C\{^1H\}$ NMR spectrum measured at this temperature also showed two C*Me* resonances (δ 22.3 and 22.2), but just one sharp signal due to the CO groups (δ 203.1, J(WC) = 166 Hz). It can be inferred from this that one molecular symmetry plane can be generated and this includes the tungsten atom, the μ_3-alkylidyne carbon atom (C(60)), and the midpoint of the Au(1)—Au(2) bond. The plausible cause of this phenomenon would involve rapid site exchange between the gold and *endo*-H atoms on both of the cage faces, accompanied by rotation of the cages about the gold atoms, while the metal core remains inflexible (Scheme 2). Somewhat related dynamic behavior has recently been reported for the argentacarborane complex [9,9′-*exo*-{$Ag(SbPh_3)_2$}$_2$-4,4′,9,9′-(μ-H)$_4$-7,7′,8,8′-*nido*-($C_2B_9H_{10}$)$_2$].[14]

The proposed process could not render the cage methyl groups on any particular cage equivalent, but ^1H and $^{13}C\{^1H\}$ NMR spectra were recorded at room temperature (21 °C), this was indeed observed to be happening, as these spectra revealed further coalescence of peaks with only one resonance for C*Me* groups appearing in both the ^1H and $^{13}C\{^1H\}$ NMR spectra (δ 1.53 (^1H) and 22.5 ($^{13}C\{^1H\}$)). Thus an additional dynamic process occurs in solution at ambient temperatures. A metal core fluxionality is proposed, where the Au–Au bond breaks so that the μ_3-CAu_2W core can flip through a planar deltahedral arrangement. The combination of the two processes in solution would be sufficient to equate all the cage methyl groups. The $^{11}B\{^1H\}$ NMR spectrum of **10a** consisted only of very broad overlapping peaks in the range δ −7.3 to −32.9.

The IR spectrum of the gold–molybdenum complex **10b** showed bands at 2059 (s) and 2018 (s) cm^{-1}. The ^1H, $^{13}C\{^1H\}$, and $^{11}B\{^1H\}$ NMR spectra of **10b** showed resonances with chemical shifts similar to those of **10a**. Furthermore, similar dynamic processes in solution were identified, as a result of variable temperature NMR experiments.

Protonation of complex **8** in thf with 1 equiv of HBF_4·Et_2O gave the neutral complex [9-*exo*-{AuW(μ-$CC_6H_3Me_2$-2,6)(CO)$_2$(η-C_5H_5)}-7,8-Me_2-*nido*-7,8-$C_2B_9H_{10}$] (**12**) in over 70% yield. The IR spectrum of the

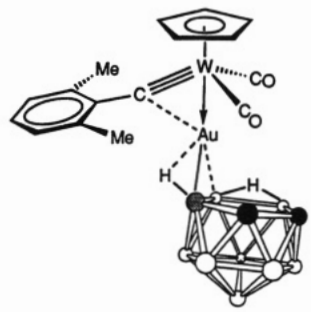

12

○ BH ◍ B ● CMe

new compound **12** showed two CO stretching bands at 2026 (vs) and 1965 (vs) cm^{-1}. In the ^1H NMR spectrum at −90 °C a very broad signal was observed at δ −2.6, integrating to one proton. This resonance is assigned to the *endo*-hydrogen atom on the *nido*-icosahedral cage face, the site of protonation. Also visible in this spectrum are two resonances arising from the cage CMe groups at δ 1.42 and 1.57, and two less-separated diagnostic shifts due to the xylyl Me_2-2,6 groups at δ 2.31 and 2.35. The non-equivalence of the various methyl groups is also displayed in the $^{13}C\{^1H\}$ NMR spectrum measured at −90 °C with pairs of peaks at δ 22.7 and 21.8 and at 22.0 and 21.7 due to the C*Me* and Me_2-2,6 nuclei, respectively. These signals were assigned on the basis of relative peak intensities of

(13) (a) Long, J. A.; Marder, T. B.; Behnken, P. E.; Hawthorne, M. F. *J. Am. Chem. Soc.* **1984**, *106*, 2979. (b) Brew, S. A.; Jeffery, J. C.; Mortimer, M. D.; Stone, F. G. A. *J. Chem. Soc., Dalton Trans.* **1992**, 1365.

(14) Park, Y.-W.; Kim, J.; Do, Y. *Inorg. Chem.* **1994**, 33, 1.

Scheme 2. Views Showing the Proposed Exchange between *endo*-Hydrogen and Cluster Gold Atoms on Either of the Carborane Cage Faces in 10a[a]

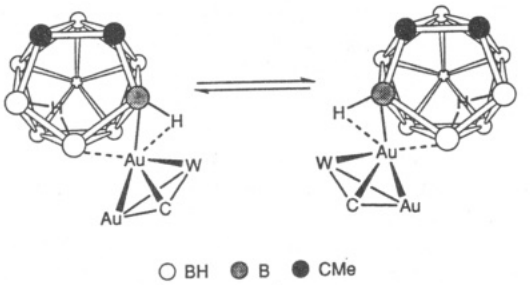

[a] Part of the cluster is omitted for clarity.

each pair and the separations observed in the ^{1}H NMR spectrum. The inequivalence of the CO ligands was also revealed in the ^{13}C{^{1}H} NMR spectrum at this temperature by the presence of two signals at δ 211.7 and 211.5 (J(WC) = 174 and 170 Hz, respectively). The μ-alkylidyne carbon nucleus resonates at δ 278.4 (J(WC) = 146 Hz), comparable with that in **8** (δ 288.6, J(WC) = 152) and complex **9** (284.3, J(WC) = 151 Hz). These low temperature data correspond to an asymmetric structure with no site exchange between the *endo*-hydrogen and the gold atom, the latter presumably occupying an exopolyhedral position similar to that of the gold atoms of compounds **10**. There may also be some weak bonding between the gold atom and the hydrogen carried by the α-boron atom, as was suggested in the structure of complex **10a**, but once again, there was no indication of this in the low temperature ^{1}H NMR spectrum of **12**. It can be inferred from these data that the xylyl group of **12** is not spinning about the μ-C–C^1(aryl) bond. The cessation of xylyl spinning, when the Me$_2$-2,6 groups would otherwise be equivalent, has been documented previously for the salt [NEt$_4$][WFe(μ-CC$_6$H$_3$-Me$_2$-2,6)(CO)$_4$(η^6-7,9-Me$_2$-7,9-C$_2$B$_{10}$H$_{10}$)].[15] A variable temperature ^{1}H NMR study of **12** was therefore prompted, focusing on the cage CMe and xylyl Me$_2$-2,6 groups. The coalescence temperature for rotation of the xylyl group about the μ-C–C^1(aryl) bond lies between −75 and −85 °C, while that for *endo*-hydrogen–gold atom exchange is within the slightly higher range −65 to −75 °C. The room temperature ^{1}H NMR spectrum of **12** shows two singlets for these groups at δ 1.46 (CMe) and 2.34 (Me$_2$-2,6), as does the ^{13}C{^{1}H} NMR spectrum at this temperature (δ 22.3 (CMe) and 21.5 (Me$_2$-2,6)). It is evident that the cage face site exchange is more facile for **12** than for the trinuclear metal complex **10a**, since this process in the latter species is more easily frozen out, with a coalescence point above ca. −40 °C. This can be credited to the additional bulk of the metal core and the extra auracarborane unit in **10a**, which are likely to be a hindrance to intramolecular mobility in solution. The room temperature ^{11}B{^{1}H} NMR spectrum of **12** revealed the usual set of broad peaks for the *nido*-icosahedral cage in the range δ −8.4 to −33.8, which must correspond to a cage where a mirror plane can be generated through the cage face β-boron and apical boron atoms and the midpoint between the C–C vertices.

The sites of protonation in complexes **3** and **8** must result from the location of uninegative charges on the *nido*-AuC$_2$B$_9$ systems, in addition to a filled orbital available for binding protons on each of the cage faces. It is interesting to note, however, that when protonation of the anion of the salt **1a** was attempted under similar conditions, only decomposition of the reagent occurred.

Treatment of a thf solution of the salt **3a** with 1 equiv of [Rh$_2$(μ-Cl)$_2$(CO)$_4$], in the presence of TlBF$_4$, yielded as the sole product the previously reported[5] cluster compound **6** in good yield (72%). Identification by IR and ^{1}H NMR spectroscopy confirmed this new synthesis of **6**. The earlier synthesis of **6** was accompanied by formation of the trinuclear metal species [WRhAu(μ-CC$_6$H$_4$Me-4)(CO)$_4$-(η-C$_5$H$_5$)(η^5-7,8-Me$_2$-7,8-C$_2$B$_9$H$_9$)], the two products being chromatographically inseparable, although crystals of **6** were grown from solutions of the mixture and the pentanuclear metal cluster thereby identified by X-ray diffraction. Thus in the new synthesis of **6** from **3a** the carborane cage is transferred from gold to rhodium as it is in the preparation of [RhAu(CO)$_2$(PPh$_3$)(η^5-7,8-Me$_2$-7,8-C$_2$B$_9$H$_9$)] (**13a**) from the reaction of the salt **1a** with [Rh$_2$(μ-Cl)$_2$(CO)$_4$].[2a]

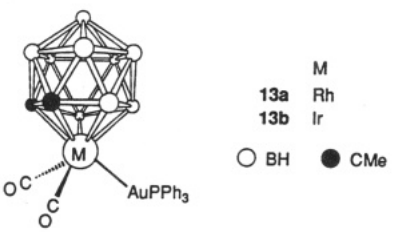

Reaction of **3a** in thf, in the presence of TlBF$_4$, with 2 equiv of [*cis*-IrCl(CO)$_2$(NH$_2$C$_6$H$_4$Me-4)] afforded the complex [WIr$_2$Au$_2$(μ_3-CC$_6$H$_4$Me-4)(CO)$_6$(η-C$_5$H$_5$)(η^5-7,8-Me$_2$-7,8-C$_2$B$_9$H$_9$)$_2$] (**14**) in low yield. Analytical, IR, and

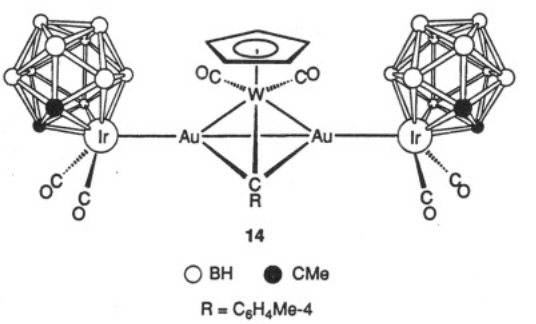

14

NMR data for this new compound (Tables 1 and 2) suggest a structure similar to that of **6**, with the same basic metal core geometry, where carborane cage transfer from gold to iridium has occurred. This synthesis is analogous to the reaction between the salt **1a** and [*cis*-IrCl(CO)$_2$-(NH$_2$C$_6$H$_4$Me-4)] which produced the iridium–gold complex [IrAu(CO)$_2$(PPh$_3$)(η^5-7,8-Me$_2$-7,8-C$_2$B$_9$H$_9$)] (**13b**).[2b] The ^{1}H NMR spectrum of **14** measured at −20 °C revealed two sharp resonances due to cage CMe groups at δ 2.52 and 2.58, with these peaks becoming slightly broader in the room temperature spectrum. A room temperature ^{13}C{^{1}H} NMR spectrum displayed a relatively low chemical shift for the μ_3-*C*C$_6$H$_4$Me-4 nucleus at δ 242.1, and four signals due to the cage CMe nuclei (δ 70.8 and 69.6 (br, *C*Me), 32.7 and 30.1 (C*Me*)). This spectrum also showed diagnostic resonances due to the carbon nuclei of the tungsten carbonyl ligands at δ 205.8 (J(WC) = 164 Hz) and the inequivalent iridium carbonyls at δ 172.6 and 172.5. There was no evidence in any spectra, including the ^{11}B NMR spectra (proton-coupled and -decoupled), of any agostic B–H→Au bonds. This is in contrast with complex **6**, the X-ray structure and ^{11}B spectra of which clearly

(15) Crennell, S. J.; Devore, D. D.; Henderson, S. J. B.; Howard, J. A. K.; Stone, F. G. A. *J. Chem. Soc., Dalton Trans* **1989**, 1363.

indicated the existence of such exopolyhedral groups.[5] This is perhaps somewhat surprising as the presence of the more electron-rich metal in the *closo*-3,1,2-IrC_2B_9 cages of **14**, in conjunction with the cage methyl groups,[2a,b] might have been expected to activate the B_β–H bonds further and promote the formation of two B–H→Au linkages.

As indicated by the room temperature ^1H NMR spectrum of **14**, some fluxional process apparently occurs just faster than the NMR time scale. A ^1H NMR spectrum measured in toluene-d_8 at 70 °C indeed showed one sharp singlet at δ 2.40 due to all the cage methyl groups. This is believed to be a further example of μ_3-CAu_2M core fluxionality, as discussed above for the species **10**, but happening within a slightly higher temperature range for **14**, with a coalescence temperature lying between 30 and 40 °C.

Conclusions

In the novel complexes **10** and **14** the carborane cage methyl groups have provided a useful NMR spectroscopic probe, not just for processes occurring on the cage face but for processes within the metal core geometry itself. It is interesting to note that no such metal core fluxionality was detected in the dianionic complex **3a**, even in NMR spectra measured up to 80 °C.

Hall and Mingos have suggested[11] that Au(I)–Au(I) contacts of the order of 3 Å may well reflect a significant bonding interaction. In the simplest of terms, it has been proposed that this can occur by donation from a filled d orbital on one gold into an empty 6p orbital of suitable symmetry on the other in a σ- or even a π-fashion. Presumably, when both the Au(I) atoms are in similar environments, a synergic bonding effect will operate. In the anion of **3a**, where there are two [*nido*-7,8-Me_2-7,8-$C_2B_9H_9$]$^{2-}$ carborane cage ligands bonded to the gold atoms, these reasonably strong electron-donating groups may reinforce the Au–Au bond by feeding in sufficient electron density to prevent fission in solution. Reduction of electron density could be achieved either by protonation, effectively generating a less powerful donor [*nido*-7,8-Me_2-7,8-$C_2B_9H_{10}$]$^-$ ligand on the gold atoms, as in the complexes **10** or by complete cage transfer from gold to iridium as in **14**. Bonding orbitals between the gold atoms might then be depopulated, lowering the activation barrier to metal core fluxionality in solution. High temperature ^1H NMR spectra of complex **6** (up to 70 °C) revealed that broadening of the peaks due to the CMe groups was beginning to occur, but not nearly to the extent of that observed for **14**. This is interpreted as greater resistance to core flexibility in **6** and may be attributed to the strengthening of the Au–Au bond by virtue of electron density supplied via the B–H→Au interactions.

Experimental Section

General Considerations. All reactions were carried out under an atmosphere of dry nitrogen, using Schlenk-line techniques. Solvents were distilled from appropriate drying agents under nitrogen before use. Celite pads used for filtration were ca. 3 cm thick. Chromatography columns (ca. 15 cm in length and 2 cm in diameter) were packed with either silica gel (Merck, 70–100 mesh) or alumina (Aldrich, Brockmann activity II). The acid HBF_4·Et_2O was used as purchased from Aldrich Chemical Co. as an 85% solution in Et_2O. The reagents [AuCl(tht)][16] and [W(≡$CC_6H_3Me_2$-2,6)$(CO)_2(\eta$-$C_5H_5)$] (**2c**)[9b,c] were made by procedures previously described. The alkylidyne complexes [M(≡CC_6H_4Me-4)$(CO)_2(\eta$-$C_5H_5)$] (M = W (**2a**), Mo (**2b**)) were prepared from the appropriate compounds [M(≡CC_6H_4Me-4)$(O_2CCF_3)(CO)_2$(pic)$_2$] (M = W, Mo; pic = 4-MeC_5H_4N),[9c] which were in turn produced by a modification of the synthesis described for [W(≡CPh)$(O_2CCF_3)(CO)_2(py)_2$] (py = pyridine) by Mayr et al.[17] The reagents [$Rh_2(\mu$-$Cl)_2(CO)_4$][18] and [*cis*-$IrCl(CO)_2(NH_2C_6H_4$Me-4)][19] were prepared by previously described methods. The NMR spectra were recorded in CD_2Cl_2 at 360 or 400 (^1H), 91 or 82 ($^{13}C\{^1H\}$), and 116 or 104 ($^{11}B\{^1H\}$) MHz.

Synthesis of the Salts [NEt_4]$_2$[10,10′-*endo*-{$Au_2M(\mu_3$-CC_6H_4Me-4)$(CO)_2(\eta$-$C_5H_5)$}-7,7′,8,8′-Me_4-*nido*-7,7′,8,8′-$(C_2B_9H_9)_2$] (M = W or Mo). (i) A suspension of Tl[*closo*-1,2-Me_2-3,1,2-$TlC_2B_9H_9$] (0.18 g, 0.31 mmol) in thf (10 mL) was cooled to −78 °C, and [AuCl(tht)] (0.10 g, 0.31 mmol) was added directly to the cooled suspension while being stirred vigorously. Over a period of ca. 5 min, a bright orange solution was formed. This mixture was stirred for a further 15 min at −78 °C, after which time **2a** (0.06 g, 0.16 mmol) was added as a solid. After 30 min the reaction mixture was warmed gradually to room temperature and [NEt_4]Cl (0.06 g, 0.36 mmol) was added. The solvent was then removed in vacuo and the residue redissolved in CH_2Cl_2 (30 mL). The resulting suspension was filtered through a Celite pad and then the solvent was removed. Crystallization from CH_2Cl_2–Et_2O (1:9, 10 mL) followed by washing with Et_2O (2 × 10 mL) and drying in vacuo, produced deep red *microcrystals* of [NEt_4]$_2$[10,10′-*endo*-{$Au_2W(\mu_3$-CC_6H_4Me-4)$(CO)_2(\eta$-$C_5H_5)$}-7,7′,8,8′-Me_4-*nido*-7,7′,8,8′-$(C_2B_9H_9)_2$] (**3a**) (0.39 g).

(ii) In a similar manner, the compounds Tl[*closo*-1,2-Me_2-3,1,2-$TlC_2B_9H_9$] (0.18 g, 0.31 mmol), [AuCl(tht)] (0.10 g, 0.31 mmol), **2b** (0.05 g, 0.16 mmol), and [NEt_4]Cl (0.06 g, 0.36 mmol) afforded deep red *microcrystals* of [NEt_4]$_2$[10,10′-*endo*-{$Au_2Mo(\mu_3$-CC_6H_4Me-4)$(CO)_2(\eta$-$C_5H_5)$}-7,7′,8,8′-Me_4-*nido*-7,7′,8,8′-$(C_2B_9H_9)_2$] (**3b**) (0.16 g) after crystallization from CH_2Cl_2–Et_2O (1:4, 10 mL), washing with Et_2O (2 × 10 mL), and drying in vacuo.

Reaction between the Compounds [WAuCl(μ-CC_6H_4Me-4)$(CO)_2(\eta$-$C_5H_5)$] and Tl[*closo*-1,2-Me_2-3,1,2-$TlC_2B_9H_9$]. A mixture of the compounds [WAuCl(μ-CC_6H_4Me-4)$(CO)_2(\eta$-$C_5H_5)$] (**7**) (0.20 g, 0.31 mmol) and Tl[*closo*-1,2-Me_2-3,1,2-$TlC_2B_9H_9$] (0.18 g, 0.31 mmol) in thf (20 mL) was stirred at room temperature while the reaction was monitored by IR spectroscopy. The reaction was complete after ca. 2 h, and [NEt_4]Cl (0.06 g, 0.36 mmol) was added. The solvent was removed in vacuo and the residue taken up in CH_2Cl_2 (30 mL). The resulting suspension was filtered through a Celite pad and the solvent again removed in vacuo. The residue was washed with Et_2O (3 × 30 mL) to remove the neutral complex **2a**. Crystallization from CH_2Cl_2–Et_2O (1:9, 10 mL), washing with Et_2O (2 × 10 mL) and drying in vacuo produced *microcrystals* of **3a** (0.38 g).

Synthesis of the Salt [NEt_4][10-*endo*-{$AuW(\mu$-$CC_6H_3Me_2$-2,6)$(CO)_2(\eta$-$C_5H_5)$}-7,8-Me_2-*nido*-7,8-$C_2B_9H_9$]. A suspension of Tl[*closo*-1,2-Me_2-3,1,2-$TlC_2B_9H_9$] (0.18 g, 0.31 mmol) in thf (10 mL) was cooled to −78 °C, and [AuCl(tht)] (0.10 g, 0.31 mmol) was added directly to the cooled suspension while being vigorously stirred. This mixture was stirred for a further 15 min at −78 °C, after which time **2c** (0.13 g, 0.31 mmol) was added as a solid. After 30 min the reaction mixture was warmed gradually to room temperature and [NEt_4]Cl (0.06 g, 0.36 mmol) added. The solvent was then removed in vacuo and the residue taken up in CH_2Cl_2 (30 mL). The resulting suspension was filtered through a Celite pad and the solvent then removed in vacuo. Crystallization from CH_2Cl_2–Et_2O (1:9, 10 mL) followed by washing with Et_2O (2 × 10 mL) produced deep orange *microcrystals* of [NEt_4][10-*endo*-{$AuW(\mu$-$CC_6H_3Me_2$-2,6)$(CO)_2(\eta$-$C_5H_5)$}-7,8-Me_2-*nido*-7,8-$C_2B_9H_9$] (**8**) (0.26 g).

Preparation of the Compounds [9,9′-*exo*-{$Au_2M(\mu_3$-CC_6H_4-Me-4)$(CO)_2(\eta$-$C_5H_5)$}-7,7′,8,8′-Me_4-*nido*-7,7′,8,8′-$(C_2B_9H_{10})_2$] (M = W or Mo). (i) The salt **3a** (0.10 g, 0.07 mmol) was dissolved

(16) Usón, R.; Laguna, A. *Organomet. Synth.* **1986**, *3*, 324.

(17) McDermott, G. A.; Dorries, A. M.; Mayr, A. *Organometallics* **1987**, *6*, 925.

(18) Cramer, R. *Inorg. Synth.* **1974**, *15*, 17.

(19) Klabunde, U. *Inorg. Synth.* **1974**, *15*, 82.

in thf (10 mL) and cooled to −78 °C. To this solution $HBF_4{\cdot}Et_2O$ (20 μL, 0.14 mmol) was added, and the reaction mixture was then warmed to room temperature over a period of 1 h with stirring. During this time the color paled from deep red to orange. Solvent was removed in vacuo, and the residue was redissolved in CH_2Cl_2 (3 mL) and chromatographed on silica gel at −20 °C. Elution with CH_2Cl_2–*n*-hexane (3:2), followed by neat CH_2Cl_2, removed a broad yellow fraction. The solvent was removed in vacuo and crystallization of the residue from CH_2Cl_2–*n*-hexane (1:5, 12 mL) yielded yellow *microcrystals* of [9,9′-*exo*-{$Au_2W(\mu_3$-CC_6H_4Me-4)$(CO)_2(\eta$-$C_5H_5)$}-7,7′,8,8′-Me_4-*nido*-7,7′,8,8′-$(C_2B_9H_{10})_2$] (**10a**) (0.05 g).

(ii) Using a similar procedure, protonation of **3b** (0.09 g, 0.07 mmol) with $HBF_4{\cdot}Et_2O$ (20 μL, 0.14 mmol) followed by chromatography on silica gel at −20 °C and crystallization from CH_2Cl_2–*n*-hexane (1:5, 12 mL) yielded yellow *microcrystals* of [9,9′-*exo*-{$Au_2Mo(\mu_3$-CC_6H_4Me-4$)(CO)_2(\eta$-$C_5H_5)$}-7,7′,8,8′-Me_4-*nido*-7,7′,8,8′-$(C_2B_9H_{10})_2$] (**10b**) (0.05 g).

Preparation of the Compound [9-*exo*-{AuW(μ-$CC_6H_3Me_2$-2,6)$(CO)_2(\eta$-$C_5H_5)$}-7,8-Me_2-*nido*-7,8-$C_2B_9H_{10}$]. The salt **8** (0.12 g, 0.14 mmol) was dissolved in thf (15 mL) and cooled to −78 °C. The reagent $HBF_4{\cdot}Et_2O$ (20 μL, 0.14 mmol) was added, and the reaction mixture was then warmed to room temperature over the course of 1 h, with stirring. A color change from deep orange to green to yellow-brown was observed during this time. The solvent was removed in vacuo, and the residue was redissolved in CH_2Cl_2 (4 mL) and chromatographed on silica gel at −20 °C. Elution was with CH_2Cl_2–*n*-hexane, initially at a ratio of 2:3 but increasing in polarity to 3:2 as a broad yellow fraction was eluted. The solvent was removed in vacuo, and crystallization of the product from CH_2Cl_2–*n*-hexane (1:4, 10 mL) gave yellow *microcrystals* of [9-*exo*-{AuW(μ-$CC_6H_3Me_2$-2,6)$(CO)_2(\eta$-$C_5H_5)$}-7,8-Me_2-*nido*-7,8-$C_2B_9H_{10}$] (**12**) (0.08 g).

Synthesis of the Complexes [$WM_2Au_2(\mu_3$-CC_6H_4Me-4$)$-$(CO)_6(\eta$-$C_5H_5)(\eta^5$-7,8-Me_2-7,8-$C_2B_9H_9)_2$] (M = Rh, Ir). (i) A mixture of the compounds **3a** (0.10 g, 0.07 mmol), $[Rh_2(\mu$-$Cl)_2$-$(CO)_4]$ (0.03 g, 0.07 mmol), and $TlBF_4$ (0.05 g, 0.16 mmol) was treated with thf (20 mL), and the resulting suspension was stirred at room temperature. After 2 h, an IR spectrum of the reaction mixture showed no further change and solvent was removed in vacuo. The residue was treated with CH_2Cl_2 (30 mL) and the suspension so formed filtered through a Celite pad. The volume of solvent was reduced in vacuo to 4 mL and this was chromatographed on alumina. Elution was with CH_2Cl_2–*n*-hexane, initially at 1:1 but increasing the polarity to 3:2, as an orange fraction was removed. The solvent was removed in vacuo, and crystallization of the solid from CH_2Cl_2–*n*-hexane (1:5, 12 mL) gave orange *microcrystals* of [$WRh_2Au_2(\mu_3$-CC_6H_4Me-4$)(CO)_6$-$(\eta$-$C_5H_5)(\eta^5$-7,8-Me_2-7,8-$C_2B_9H_9)_2$] (**6**) (0.08 g, 72% yield).

(ii) To a mixture of the compounds **3a** (0.18 g, 0.13 mmol), [*cis*-$IrCl(CO)_2(NH_2C_6H_4$Me-4$)$] (0.10 g, 0.26 mmol), and $TlBF_4$ (0.08 g, 0.29 mmol) was added thf (20 mL), and the resulting suspension was stirred at room temperature. After 3 h, the IR spectrum of the reaction mixture showed no further change, so the solvent was removed in vacuo. To the residue was added CH_2Cl_2 (30 mL) and the suspension filtered through a Celite pad. The volume of the solvent was reduced in vacuo to ca. 4 mL and this was chromatographed on alumina at −20 °C. A broad yellow fraction was eluted with CH_2Cl_2–*n*-hexane (2:3) and solvent was then removed in vacuo. Crystallization from CH_2Cl_2–*n*-hexane (1:4, 10 mL) gave orange *microcrystals* of [WIr_2-$Au_2(\mu_3$-CC_6H_4Me-4$)(CO)_6(\eta$-$C_5H_5)(\eta^5$-7,8-Me_2-7,8-$C_2B_9H_9)_2$] (**14**) (0.07 g).

Crystal Structure Determinations. The crystal data and experimental parameters for compounds **8** and **10a** are given in Table 5. Crystals of **8** were grown by diffusion of Et_2O into a CH_2Cl_2 solution of the complex. The crystal used for data collection was mounted in a sealed glass capillary under N_2. Crystals of **10a** were grown by diffusion of *n*-hexane into a CH_2Cl_2 solution of the complex. The complex crystallizes with a molecule of CH_2Cl_2 in the asymmetric unit and solvent loss occurs fairly rapidly if the crystals are removed from solution. The crystal used for data collection was mounted in a sealed glass capillary under N_2 saturated with CH_2Cl_2–*n*-hexane (ca. 1:4). During data collection, three check relfections showed a gradual loss of intensity and decay to ca. 70% of their initial values by the time collection was completed. This decay may well have been associated with the loss of CH_2Cl_2 from the crystal lattice, but this did not prevent the completion of data collection. All data were corrected for Lorentz, polarization, and X-ray absorption effects, the last by an empirical method based upon ψ data.[20] The structures were solved by conventional heavy atom methods, and successive Fourier difference syntheses were used to locate all non-hydrogen atoms.

Table 5. Crystallographic Data[a]

compd	**8**	**10a**
cryst dimens/mm	0.82 × 0.30 × 0.25	0.40 × 0.35 × 0.28
formula	$C_{28}H_{49}AuB_9NO_2W$	$C_{23}H_{44}Au_2B_{18}O_2W{\cdot}CH_2Cl_2$
M_r	909.8	1209.9
cryst color, shape	orange prism	yellow prism
cryst system	monoclinic	monoclinic
space group	$P2_1/c$	$P2_1/c$
a/Å	8.741(3)	16.676(4)
b/Å	21.100(5)	13.879(5)
c/Å	19.300(5)	18.260(6)
β/deg	98.33(2)	90.90(2)
V/Å^3	3522(2)	4225(2)
Z	4	4
d_{calcd}/g cm^{-3}	1.72	1.90
μ(Mo Kα)/cm^{-1}	74.5	97.9
F(000)/e	1752	2248
2θ range/deg	4–50	4–50
no. of reflns meas	6838	8076
no. of unique reflns	6200	7450
no. of obsd reflns	4743	3770
criterion for data used [$F_o \geq n\sigma(F_o)$]	$n = 5$	$n = 4$
R (R')[b]	0.054 (0.052)	0.057 (0.056)
S (goodness-of-fit)	1.63	1.42
final electron density diff features (max/min)/e Å^{-3}	2.31/−3.13	1.07/−1.15

[a] Data collected at 293 K on a Siemens R3m/V four-circle diffractometer operating in the Wyckoff ω-scan mode; graphite monochromated Mo Kα X-radiation, λ = 0.710 73 Å. Refinement was by full-matrix least squares on F with a weighting scheme of the form $w^{-1} = [\sigma^2(F_o) + g|F_o|^2]$ with $g = 0.0008$ (**8**) and 0.0005 (**10a**) where $\sigma^2(F_o)$ is the variance in F_o due to counting statistics; g was chosen so as to minimize variation in $\sum w(|F_o| - |F_c|)^2$ with $|F_o|$. [b] $R = \sum||F_o| - |F_c||/\sum|F_o|$, $R' = \sum w^{1/2}||F_o| - |F_c||\sum w^{1/2}|F_o|$.

For **8** all non-hydrogen atoms were refined with anisotropic thermal parameters. Methyl, methylene, xylyl, and cyclopentadienyl hydrogen atoms were included in calculated positions (C–H = 0.96 Å) with fixed isotropic thermal parameters (U_{iso} = 0.08 Å^2). Terminal B—H hydrogen atoms were also included in calculated positions [B—H = 1.1 Å, $U_{iso} = 1.2U_{eq}$(B)].[21] The large difference map features in the final difference Fourier synthesis were located close to the metals and absorption problems were probably exacerbated by the use of a large crystal.

For **10a** all non-hydrogen atoms were refined with anisotropic thermal parameters and the tolyl and cyclopentadienyl rings were treated as rigid groups. The anisotropic thermal parameters for these non-hydrogen atoms, including those of the metals were observed to be unusually large. This is believed to reflect the fairly high degree of thermal activity experienced by the constituent atoms of this complex, a phenomenon indicated by the sudden decrease in the intensities of reflections beyond 2θ ≈ 40°. In addition, one molecule of CH_2Cl_2 occupies the asymmetric unit and its atomic anisotropic thermal parameters are also large. Methyl, methylene, and aromatic hydrogen atoms were included in calculated positions (C—H = 0.96 Å) with fixed isotropic thermal parameters (U_{iso} = 0.10 Å^2). Exopolyhedral B—H hydrogen atoms, except those bound to B(3) and B(16), were also included in calculated positions [B—H = 1.1 Å, $U_{iso} = 1.2U_{eq}$(B)].[21] The B–H–B bridging hydrogen atoms H(1) and

(20) Sheldrick, G. M. SHELXTL-PC programs for use with the Siemens X-Ray System. Siemens, Madison, WI.

(21) Sherwood, P. BHGEN, a program for the calculation of idealized H-atom positions for a *nido*-icosahedral carborane cage. University of Bristol, 1986.

Table 6. Atomic Coordinates (×10⁴) and Equivalent Isotropic Displacement Parameters (Å² × 10³) for 8

	x	y	z	U(eq)[a]		x	y	z	U(eq)[a]
Au	1850(1)	887(1)	2811(1)	54(1)	W	1580(1)	987(1)	4181(1)	55(1)
C(1)	4442(12)	1137(5)	1988(6)	60(4)	C(2)	3945(13)	1814(5)	2216(7)	68(4)
B(3)	2072(15)	1890(6)	2132(8)	62(5)	B(4)	1188(15)	1180(6)	1746(7)	57(4)
B(5)	2981(14)	670(6)	1764(7)	58(4)	B(6)	4734(14)	1759(7)	1446(8)	65(5)
B(7)	3131(17)	2251(6)	1509(8)	71(5)	B(8)	1468(16)	1833(6)	1199(8)	66(5)
B(9)	2011(14)	1039(6)	932(7)	59(4)	B(10)	4068(15)	1014(6)	1124(8)	63(4)
B(11)	3123(16)	1722(7)	775(8)	69(5)	C(10)	5902(13)	853(6)	2377(8)	78(5)
C(20)	4937(17)	2146(6)	2796(7)	88(5)	C(3)	1906(13)	317(6)	4910(7)	69(4)
O(3)	2136(12)	-89(5)	5297(5)	96(4)	C(4)	3868(14)	1122(6)	4330(8)	76(5)
O(4)	5149(10)	1212(5)	4426(6)	103(4)	C(50)	975(18)	1841(7)	4878(9)	96(6)
C(51)	-209(17)	1411(7)	4825(8)	81(5)	C(52)	-916(14)	1410(6)	4143(8)	77(5)
C(53)	-107(16)	1810(6)	3742(8)	80(5)	C(54)	1120(19)	2073(6)	4230(11)	100(7)
C(60)	1670(10)	243(5)	3628(5)	51(3)	C(61)	1646(11)	-431(5)	3457(6)	54(3)
C(62)	3003(13)	-796(6)	3579(8)	73(5)	C(63)	2905(17)	-1449(6)	3472(9)	94(6)
C(64)	1537(17)	-1735(6)	3253(9)	93(6)	C(65)	218(16)	-1379(6)	3115(8)	87(5)
C(66)	229(13)	-721(5)	3208(7)	67(4)	C(67)	-1201(13)	-342(7)	3031(9)	91(6)
C(68)	4535(13)	-480(7)	3816(9)	93(6)	N	7237(11)	1247(4)	-593(6)	68(4)
C(701)	6014(30)	1190(14)	-1126(16)	305(21)	C(702)	4582(22)	1172(10)	-1349(13)	168(12)
C(703)	6968(25)	556(8)	-295(12)	133(10)	C(704)	7882(17)	374(6)	338(7)	85(5)
C(705)	8740(26)	1287(15)	-718(14)	215(18)	C(706)	9611(25)	1002(11)	-1154(13)	176(14)
C(707)	6882(27)	1699(10)	-141(17)	238(19)	C(708)	6716(24)	2360(6)	-200(10)	126(9)

[a] Equivalent isotropic U defined as one-third of the trace of the orthogonalized U_{ij} tensor.

Table 7. Atomic Coordinates (×10⁴) and Equivalent Isotropic Displacement Parameters (Å² × 10³) for 10a

	x	y	z	U(eq)[a]		x	y	z	U(eq)[a]
W	2325(1)	2424(1)	750(1)	75(1)	Au(1)	1621(1)	1584(1)	-436(1)	69(1)
Au(2)	3414(1)	1989(1)	-298(1)	78(1)	C(1)	2025(14)	-779(21)	-1648(15)	125(12)
C(2)	1605(12)	-672(14)	-904(10)	82(8)	B(3)	1046(12)	285(17)	-847(11)	69(8)
B(4)	1089(16)	936(20)	-1695(12)	88(10)	B(5)	1812(23)	132(29)	-2225(18)	141(17)
B(6)	1254(18)	-1558(21)	-1498(17)	116(13)	B(7)	581(13)	-878(17)	-992(13)	80(9)
B(8)	285(13)	120(19)	-1518(14)	92(11)	B(9)	813(21)	52(32)	-2379(14)	149(19)
B(10)	1388(24)	-1017(27)	-2316(19)	145(18)	B(11)	433(15)	-1042(22)	-1953(14)	104(12)
C(10)	2866(14)	-1243(20)	-1673(20)	241(24)	C(20)	2059(15)	-1000(19)	-248(14)	152(14)
C(3)	5322(13)	2148(18)	-684(12)	100(10)	C(4)	5468(14)	2727(15)	-1394(14)	109(11)
B(14)	4720(16)	2468(21)	-1984(14)	100(12)	B(15)	4089(13)	1561(21)	-1544(14)	91(10)
B(16)	4575(13)	1514(23)	-673(12)	98(12)	B(17)	6073(14)	1883(23)	-1251(17)	110(13)
B(18)	5689(16)	2019(24)	-2107(15)	111(13)	B(19)	4853(16)	1277(22)	-2222(13)	102(12)
B(20)	4764(16)	595(19)	-1357(14)	102(12)	B(21)	5529(15)	986(21)	-802(16)	105(13)
B(22)	5711(17)	898(22)	-1722(16)	115(13)	C(30)	5528(16)	2725(22)	20(16)	181(18)
C(40)	5689(14)	3803(17)	-1328(16)	164(16)	C(5)	2951(19)	3628(22)	872(14)	136(14)
O(5)	3342(13)	4305(16)	965(12)	178(11)	C(6)	1352(15)	3249(24)	768(13)	126(14)
O(6)	775(12)	3700(15)	736(10)	149(10)	C(51)	1788(11)	1195(15)	1463(10)	102(11)
C(52)	1827	2028	1914	125(14)	C(53)	2646	2289	2004	126(13)
C(54)	3113	1617	1608	121(13)	C(55)	2583	941	1274	99(10)
C(60)	2347(10)	2809(13)	-303(10)	76(8)	C(61)	2286(10)	3583(9)	-875(7)	74(8)
C(62)	1537	3810	-1179	89(9)	C(63)	1460	4580	-1666	93(10)
C(64)	2132	5122	-1849	89(9)	C(65)	2881	4895	-1545	94(10)
C(66)	2958	4125	-1058	102(10)	C(67)	2064(13)	5989(15)	-2367(10)	104(10)
C(70)[b]	912(25)	6178(30)	371(29)	352(44)	Cl(1)[b]	594(7)	7213(10)	735(7)	240(7)
Cl(2)[b]	1902(10)	6067(11)	219(8)	301(9)					

[a] Equivalent isotropic U defined as one-third of the trace of the orthogonalized U_{ij} tensor. [b] Solvent molecule.

H(2) were located in a final electron density difference synthesis and were refined with fixed isotropic thermal parameters (U_{iso} = 0.10 Å²). The B—H hydrogen atoms H(3) and H(16) were also located in a final electron density difference synthesis and were refined with constrained B—H bond distances [B(3)—H(3) and B(16)—H(16) = 1.1(1)Å] and fixed isotropic thermal parameters (U_{iso} = 0.10 Å²). It was deemed necessary to locate these particular two hydrogen atoms and not rely on the terminal B—H hydrogen calculation program because the latter assumes a *closo*-icosahedral cage geometry where the metal is ideally on or close to one of the vertices. The gold atoms Au(1) and Au(2), which are chiefly bound to the boron atoms B(3) and B(16), respectively, occupy essentially exopolyhedral sites, and the B(3)—H(3) and B(16)—H(16) bonds were expected to be displaced from the B–H vectors where they would be observed in a more regular *closo*-icosahedron. Because of the partial solvent loss, the structural parameters for **10a** should be treated with due caution.

All computations were performed on a DEC μ-Vax II computer with the SHELXTL system of programs.[20] Atomic scattering factors with corrections for anomalous dispersion were taken from ref 22, and final atomic positional parameters (x, y, z, U(eq)s) for non-hydrogen atoms are listed in Tables 6 and 7.

Acknowledgment. We thank the U.K. Science and Engineering Research Council for the award of a research studentship (to P.A.J.) and the Robert A. Welch Foundation for support (Grant AA-1201).

Supplementary Material Available: Complete tables of bond lengths and angles, anisotropic thermal parameters, and hydrogen atom parameters for **8** and **10a** (21 pages). Ordering information is given on any current masthead page.

OM9401667

(22) *International Tables for X-ray Crystallography*; Kynoch Press; Birmingham, U.K., 1974; Vol. 4.